Seawater effects on properties of bentonite cut-off walls with/without cement addition

Wentao Li[a], Matthew Zhi Yeon Ting[b], Junde Qin[c], and Yaolin Yi[d]*

[a]Assistant Professor, School of Rail Transportation, Soochow University, Suzhou, 215131, P. R. China. Email: wtli2022@suda.edu.cn

[b]Research Fellow, School of Civil and Environmental Engineering, Nanyang Technological University, 639798, Singapore. Email: matthewzhiyeon.ting@ntu.edu.sg

[c]Research Fellow, School of Civil and Environmental Engineering, Nanyang Technological University, 639798, Singapore. Email: Junde002@e.ntu.edu.sg

[d]Associate Professor, School of Civil and Environmental Engineering, Nanyang Technological University, 639798, Singapore. Email: yiyaolin@ntu.edu.sg (*corresponding author).

Abstract: Bentonite-based cut-off walls have been widely used to protect coastal areas against seawater intrusion. However, salts contained in coastal soils affect properties of bentonite cut-off walls, and interactions between seawater and bentonite minerals with or without cement remain unclear. Therefore, this study aims to evaluate seawater effects on the workability, strength, and permeability of bentonite-based mixtures, prepared using three types of bentonite, namely sodium, calcium, and seawater bentonite. The underlying mechanisms were further investigated through Atterberg limits, mineralogical, and microstructural analyses. Results show that the cation exchange between seawater and bentonite leads to alterations in montmorillonite type and particle arrangement. This leads to a significantly reduced liquid limit and a slightly decreased plastic limit of bentonite, therefore narrowing the range of workable water content for bentonite-sand mixtures. Compared with sodium/calcium bentonite, the seawater bentonite is less impacted by seawater, but shows a larger increment in workability after cement addition due to palygorskite dissolution. Under similar workability, the bentonite-sand-cement mixture with calcium bentonite yields the highest strength and the lowest permeability. These

findings illustrate correlations between bentonite mineral alternations and properties of bentonite-sand mixtures with or without cement, and offer guidance for cut-off walls construction in coastal regions.

Keywords: Bentonite; seawater; workability; permeability; cation exchange

1. Introduction

Sea-level rise has accelerated in recent decades. Consequently, the average sea-level is projected to rise by about 0.3 m by 2050 and 0.6–1.1 m by 2100 (Vernimmen and Hooijer, 2023, Boesch et al., 2018). Coastal areas, especially the low-lying islands and coasts, are vulnerable to this change. Driven by the difference in water levels on either side of the seawall or dike, seawater can easily penetrate through the permeable sand layer, and this issue will become increasingly critical with the rising sea-level. The construction of low permeable seepage barriers, i.e., cut-off walls, is one of the effective techniques in intercepting seawater intrusion through the highly permeable sand layer.

Seepage cut-off walls are often installed in porous soil layers, particularly sand, and are extended into an impervious stratum or bedrock to reduce seepage. During the installation, bentonite and water are blended with in-situ soils to yield a slurry-form mixture, in which bentonite controls the rheological behavior and is responsible for minimizing permeability (Shi et al., 2022). Cement slurry can be injected into and remixed with the homogeneous sand-bentonite mixture, aiming to further enhance the strength and reduce the permeability. The fresh slurry-state mixture should meet the workability requirements for flowability and bleeding. Specifically, the flowability of fresh mixture should be in the range of 150-230 mm using the flow table method (Evans, 2007), and the bleeding value is suggested to be less than 3% (JCJ/T303, 2013). For the hardened cement-bentonite cut-off walls, the requirement of permeability coefficient is commonly designed to be within 1×10^{-8} cm/s (Wu et al., 2021). However, for cut-off walls installed in coastal regions, the presence of sea salts in in-situ soils and the infiltration of seawater lead to the interactions between salts and bentonite. The effects of seawater or saline solution on the properties of bentonite have been examined. Ying et al. (2021) indicated that the diffuse double layer of

montmorillonite, was significantly depressed after being exposed to salty water due to cation exchange, resulting in a decreased swelling capacity of bentonite. As a result, the workability of bentonite-sand mixtures might increase significantly, posing challenges to constructability and contributing to solid-liquid separation and heterogeneity of bentonite-sand walls. For cement-bentonite-sand cut-off walls, cement hydrates upon mixing with water, which releases an excessive amount of Ca^{2+} ions. The interaction between Ca^{2+} ions and bentonite affects the swelling ability of bentonite (Kaufhold et al., 2020), thereby altering the constructability of cement-sand-bentonite mixtures (Cheng et al., 2022). In the presence of seawater, the aggressive ions induced by seawater can react with both bentonite and cementitious materials, affecting not only the short-term workability, but also the long-term permeability of the cement-sand-bentonite mixture. Therefore, it is of great significance to investigate seawater effects on properties of bentonite-based cut-off walls, which can provide support for the construction of bentonite-based cut-off walls in coastal areas.

Using bentonite with high salt-resistance capacity is a potential solution to mitigate the seawater effects on bentonite-based cut-off walls. Bentonite has been commonly categorized into sodium or calcium bentonite, depending on its predominantly montmorillonite types. Mishra et al. (2009) and Shi et al. (2022) suggested that calcium bentonite showed higher chemical stability than sodium bentonite when exposed to NaCl and CaCl solutions, respectively. Thus, calcium bentonite might be an alternative to sodium bentonite in marine regions by minimizing the impact of seawater-induced cation exchange. Existing studies have also attempted to use bentonite containing salt-resistant components in seawater environments. Palygorskite is a magnesium-alumina silicate (Simpson et al., 2021) which shows high salt-resistance capacity. The work of Cui et al. (2020) indicated that the blends of palygorskite and bentonite outperform conventional bentonites against salt impacts, and palygorskite bentonite compounds have been employed in coastal engineering operations, such as drilling and tunneling (Choupani et al., 2022). Compared with sodium bentonite, although calcium bentonite and salt-resistant bentonite were less affected by seawater, their applications in coastal cut-off walls require further investigation. To the author's best knowledge, no research has been conducted on the performance of

cement-bentonite cut-off walls with different bentonite types and coupled influence of seawater and cement hydration.

Therefore, this study investigated the properties of bentonite-based cut-off walls with the use of both seawater and deionized water. Three types of bentonite, i.e., sodium bentonite, calcium bentonite, and bentonite containing salt-resistant components, were used to investigate the effects of bentonite mineralogy on the resistance to seawater. The flowability and bleeding of fresh mixtures were evaluated, and the permeability and strength of hardened mixtures were tested after 56 days of curing. Mineralogical, chemical, and microstructural analyses, including X-ray diffraction (XRD), Fourier-transform infrared spectroscopy (FTIR), and scanning electron microscope (SEM), were also performed.

2. Materials and methods

2.1. Materials

Three types of bentonite, namely sodium bentonite (Na_B), calcium bentonite (Ca_B), and seawater bentonite (SW_B), were utilized in this study. The Na_B, Ca_B, and SW_B were obtained from International Scientific Pte. Ltd., Singapore, Guangzhou Changying Trading Co. Ltd., China, and Yeochem (S) Pte. Ltd., Singapore, respectively. The unit price of Na_B, Ca_B, and SW_B were 1, 0.64, and 1.52 SGD per kg, respectively. The Na_B and Ca_B were categorized based on their primary exchangeable cation type. As shown in Table 1, the geotechnical and physiochemical properties of these bentonites were evaluated as per ASTM D4318 (ASTM, 2017) and ASTM D7508 (ASTM, 2018). Results showed that Na_B had the highest liquid limit (403%), followed by Ca_B (242%) and SW_B (204%). The Na_B had 53.14 cmol/kg of exchangeable Na^+ cation, while that of Ca_B and SW_B was 43.63 and 4.41 cmol/kg, respectively.

The particle size distribution of sand is shown in Figure 1. Artificial seawater with 3% salinity was produced by adding sea salt to deionized water for reproducing the marine environment approximately to Singapore (Kumar et al., 2019). Ordinary Portland cement, purchased from Engro Pte. Ltd. Singapore, was used. Table 2 shows the chemical

composition of these materials determined by X-ray fluorescence technique. As shown in Table 2, Na_B had the lowest calcium content and the highest sodium percentage. The SW_B had significantly higher calcium and magnesium contents compared with other types of bentonites.

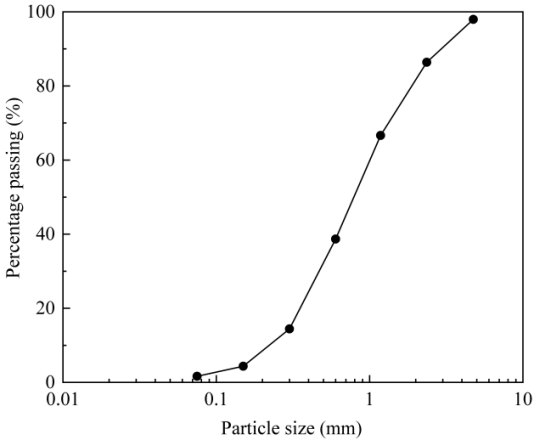

Figure 1. Particle size distribution of sand

Table 1. Fundamental properties of bentonites

Properties		Na_B	Ca_B	SW_B
Specific gravity		2.69	2.71	2.15
Plastic limit (%)		58	43	87
Liquid limit (%)		403	242	204
Plasticity index (%)		345	199	117
Exchangeable cation (cmol/kg):	Na^+	53.14	43.63	4.41
	K^+	0.43	0.75	0.16
	Ca^{2+}	19.25	37.57	34.65
	Mg^{2+}	0.29	1.02	2.68

Table 2 Chemical composition (wt %) of materials

Material	CaO	SiO_2	MgO	Al_2O_3	Fe_2O_3	SO_3	K_2O	Na_2O	Cl	Others
Na_B	1.76	61.51	1.79	10.77	18.29	0.15	ND	2.84	ND	2.89
Ca_B	3.76	69.77	2.51	12.45	5.70	0.04	1.62	2.76	ND	1.39
SW_B	13.91	63.18	11.79	5.41	3.99	0.06	0.27	0.33	ND	1.06
Cement	70.21	15.63	1.69	4.83	3.16	3	0.68	ND	ND	0.80
Sea salt	2.72	ND	13.73	ND	ND	16.1	2.14	19.9	44.4	1.01

ND-not detected.

2.2. Mixture preparation and testing program

Table 3 shows the experiment program of bentonite-sand mixtures. Bentonite content, defined as the bentonite-to-sand ratio by mass, was chosen to be 4%, 8%, and 12% with reference to existing research (Evans and Garbin, 2009, Norris et al., 2018). To prepare the bentonite-sand mixture, solids were weighed and mixed in a blender for 5 minutes. Afterwards, deionized water or seawater was poured into the blender and mixed for another 5 minutes before testing for workability. For the cement-bentonite-sand mixture, fresh cement slurry with a liquid/solid ratio of 1.0 was mixed with the sand-bentonite mixture for another 5 minutes. The cement content used in this study was selected to be 10% (Cheng et al., 2022). This process attempted to reproduce the cut-off wall construction in two phases, i.e., bentonite slurry mixing (first phase) and cement slurry mixing (second phase). The flowability and bleeding tests were then performed for the fresh cement-bentonite-sand mixture.

For the flowability test, the homogeneous mixture was poured into a flow mold placed in the flow table center. Afterwards, the mold was lifted away from the mixture and then the flow table was lifted and dropped vertically 25 times within 15 seconds. Afterwards, the diameter of mixtures was recorded four times to determine the average value of these diameters, i.e., the flow value. The bleeding of the mixture was then evaluated (ASTM, 2016). The mixture of 800 ± 10 mL was poured into a graduated cylinder with a total capacity of 1000 mL. The volumes of bleeding water and the total mixture were then recorded for up to 24 hours to determine the bleeding rate. The cement-bentonite-sand mixtures were cast into cylindrical molds for strength and permeability tests. The specimens inside mold were sealed within ziplock bags for 28 days. Afterwards, hardened specimens were demolded, and specimens prepared with deionized water or seawater were then cured in deionized water or seawater respectively for an additional 28 days. The strength and permeability of these samples were tested after a curing age of 56 days as per ASTM standards (ASTM, 2010, ASTM, 2007). The mixture design and testing program are shown in Table 3. Selected bentonite mixtures were collected and sieved for XRD, FTIR, and SEM tests after freeze-drying.

Table 3 Mixture design and testing program

Bentonite	Bentonite content	Water type	Water content	Cement content	Tests
Na_B, Ca_B, and SW_B	4%, 8%, and 12%	Deionized water and seawater	20%-80%	0 and 10%	Flowability, bleeding, strength, permeability, Atterberg limits, XRD, SEM, and FTIR

3. Results and analysis

3.1 Workability of bentonite-sand mixture

The flowability of bentonite-sand mixture using deionized water or seawater was plotted in Figure 2. Please note that the diameter of the flow table used in this study is 254 mm, and hence a flow value of 254 mm means that the sample overflowed. For all the bentonite types, when a higher bentonite content was used, the water content range for mixtures to remain a desirable flowability, i.e., the workable water content range, was extended. Taking Na_B mixture as an example, its water content should remain in the range of 32%-42% to achieve a desirable flowability with 4% bentonite content when using deionized water, while this range increases to 60%-78% with 12% bentonite content.

The water type has a critical impact on the flowability of bentonite-sand mixtures. For the bentonite-sand mixture with 4% bentonite content and 30% water content, the increment in flowability was 64% for Na_B mixture (from 120 to 197 mm), 40% for Ca_B mixture (from 143 to 200 mm), and 21% for SW_B mixture (from 159 to 193 mm) when deionized water was replaced by seawater. Thus, the workable water content range decreased significantly. For instance, the workable water content range of bentonite-sand mixture with 12% Na_B decreased from 60%-78% to 32%-42% (Figure 2a) when seawater rather than deionized water was used. A similar observation was noticed for Ca_B mixture, as the acceptable water content range decreased from 55%-73% to 32%-42%. However, for the mixture containing 12% SW_B, this range changed slightly from 42%-49% to 37%-45%.

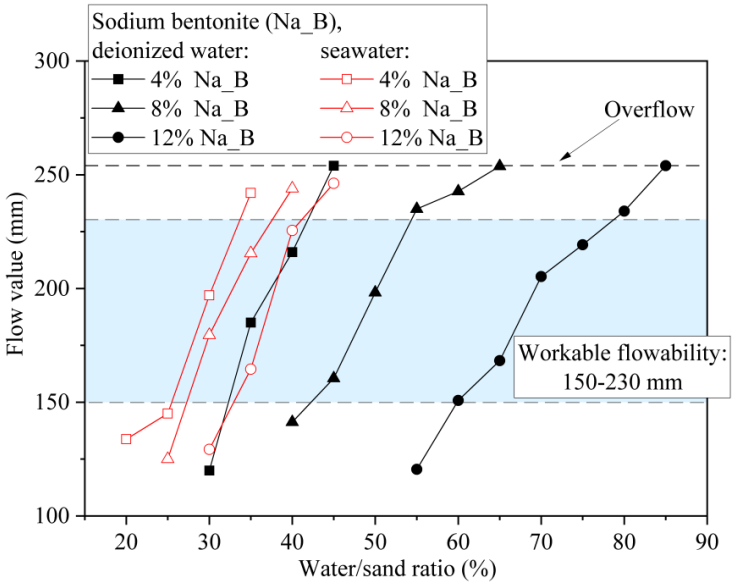

185

186 (a)

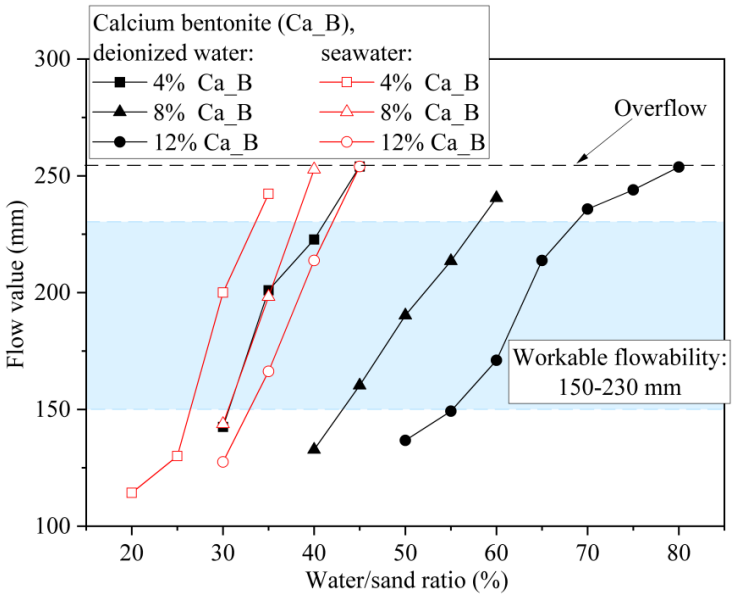

187

188 (b)

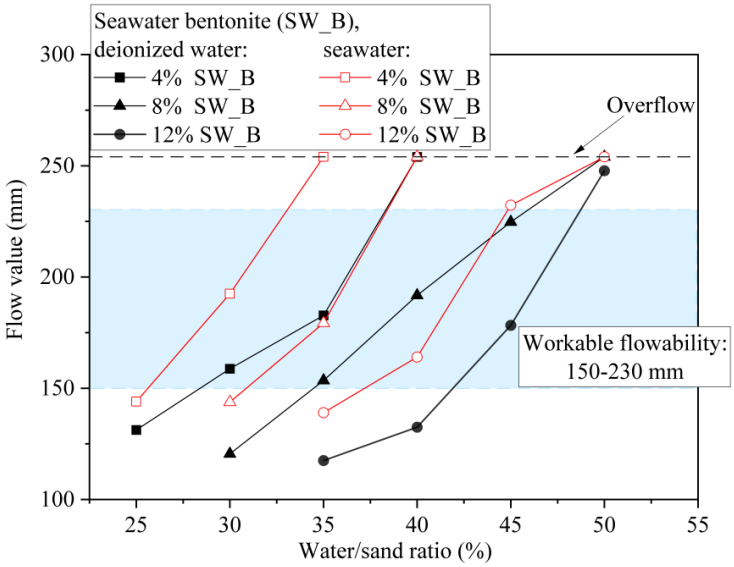

(c)

Figure 2. Flow value of bentonite-sand mixtures with addition of seawater and deionized water: (a) Na_B, (b) Ca_B, and (c) SW_B

For bentonite-sand mixtures that met flowability requirements, their bleeding rate was evaluated and plotted in Figure 3. For all mixtures, the bleeding increased with water-to-sand ratio, which is similar to that of the flowability results as shown in Figure 2. When deionized water was used, Na_B was more efficient in decreasing the bleeding of bentonite-sand mixture compared with Ca_B and SW_B due to its higher liquid limit. When seawater was used, there was a remarkable increase in the bleeding rate of mixtures containing either Na_B or Ca_B, indicating a reduced water-holding capacity of the bentonite. The bleeding of SW_B mixtures also increased in the seawater environment, but the increment was less prominent compared with that of Na_B or Ca_B mixtures. For bentonite-sand mixtures with an acceptable flow value, their bleeding rate is lower than 3%. In summary, the seawater effect on the flowability and bleeding is more significant for mixtures containing Na_B/Ca_B when compared with the SW_B.

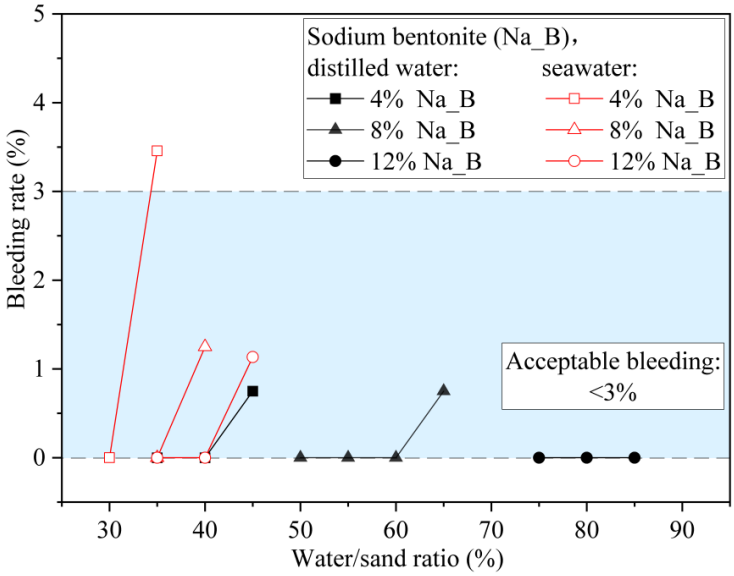

206

207 (a)

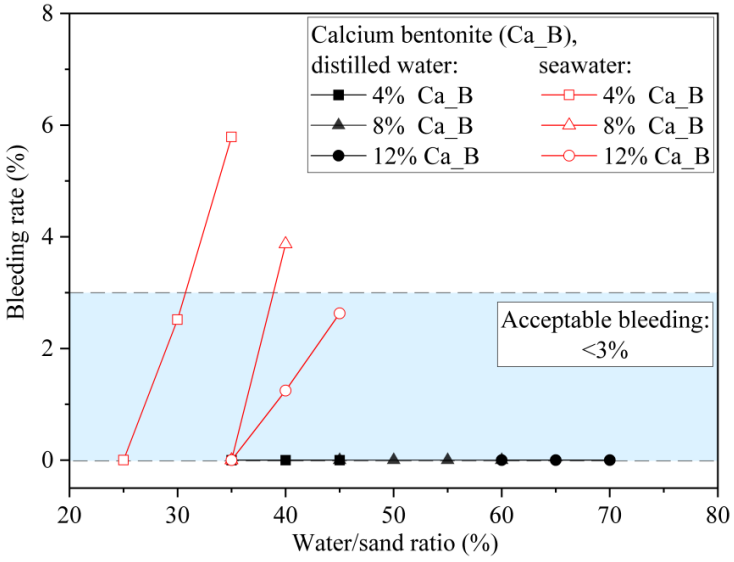

208

209 (b)

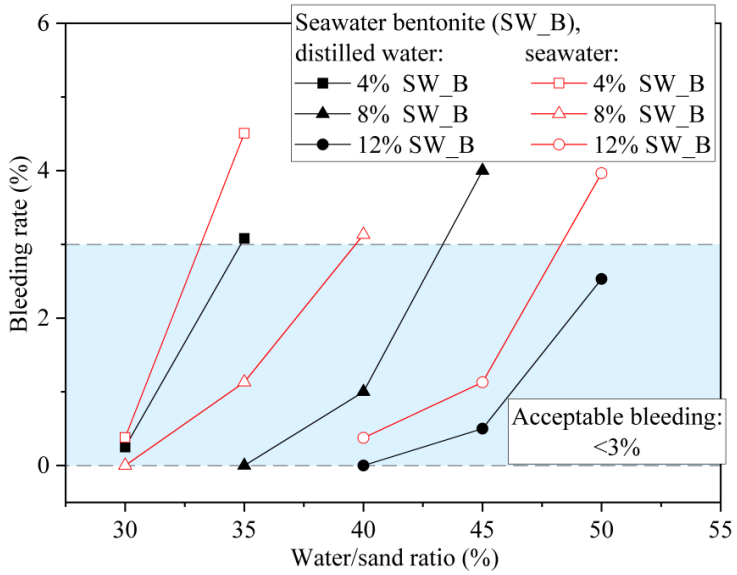

(c)

Figure 3. Bleeding rate of bentonite-sand mixtures with addition of seawater and deionized water: (a) Na_B, (b) Ca_B, and (c) SW_B

3.2 Properties of cement-bentonite-sand mixture

Sand-bentonite mixtures within the acceptable workability range were selected for adding cement slurry. As shown in Figure 4, adding cement slurry led to an increase in flowability. This could be attributed to two reasons. Firstly, the flowability of cement slurry (>254 mm) was higher than that of bentonite-sand mixtures. Secondly, Ca^{2+} cations induced by cement slurry could also interact with bentonite, which further lowers the water-retention capacity of bentonite and hence the increasing flowability. It is noticed that cement effect on the flowability of deionized water-blended mixtures was less prominent compared with those of seawater-blended mixtures.

As shown in Figure 5, adding cement slurry showed an insignificant influence on the bleeding rate of mixtures containing Na_B or Ca_B. This is because the hydration of cement occurs after mixing and continuously produces cementitious materials, bridging sand and bentonites together and hence hindering the solid-liquid segregation, i.e., the bleeding. While for the SW_B mixture, the effects of adding cement slurry were evident. Cement addition increased the bleeding of SW_B mixture by 2%, while this value was

around 1% for the Na_B or Ca_B mixture. Compared with the Na_B and Ca_B mixture, the workability of SW_B mixture was less affected by seawater, but it was susceptible to the detrimental influences of cement slurry.

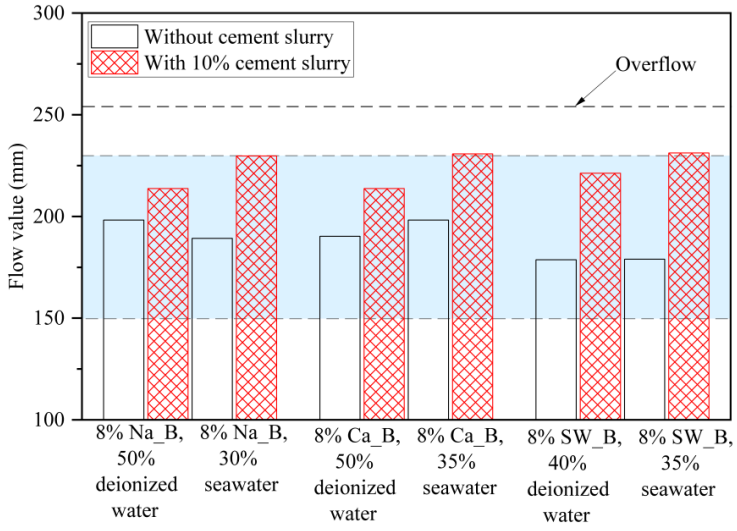

Figure 4. Flow value of bentonite-sand mixtures with/without addition of cement slurry

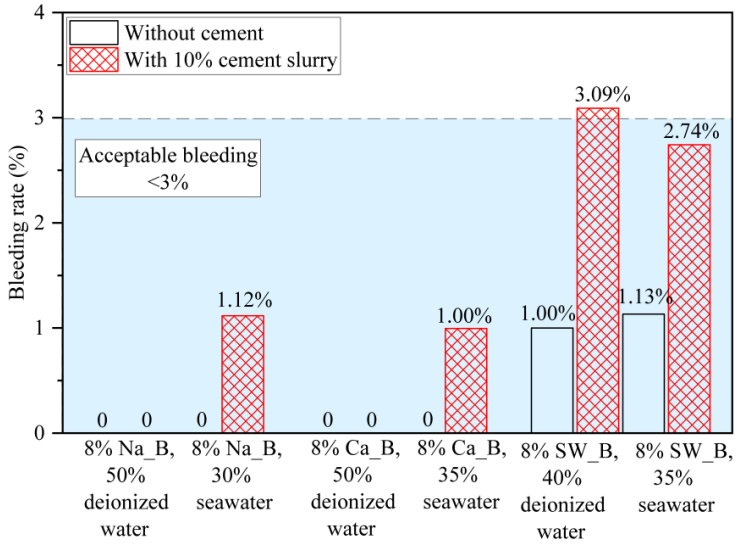

Figure 5. Bleeding rate of bentonite-sand mixtures with/without addition of cement slurry

The unconfined compressive strength (UCS) of cement-bentonite-sand mixtures at 56 days is shown in Figure 6. It was found that specimens prepared with seawater had a higher UCS than the corresponding specimen mixed with deionized water. This is because the seawater-mixed specimens had a water content 5%-15% lower than that of the deionized-mixed ones, leading to a relatively denser microstructure and hence a higher strength. Additionally, seawater could facilitate cement hydration, contributing to the strength development. The Ca_B mixtures had the highest UCS among the three types of bentonites with the same cement content, while mixtures containing SW_B had the lowest UCS at 56 days, even with a 0-10% lower water content. Take the specimens with 8% bentonite and 35% seawater as an example, the strength of Ca_B mixture was 4.4 times higher than that of the SW_B mixture. The strength of SW_B mixture with 40% deionized water was even slightly lower than the Na_B mixture with 50% deionized water. This may be because the SW_B has the highest magnesium content, which reacted with hydration products to form magnesium hydroxide (MH) and non-cementing magnesium silicate hydrate (MSH) (Bernard et al., 2019), leading to a relatively low strength.

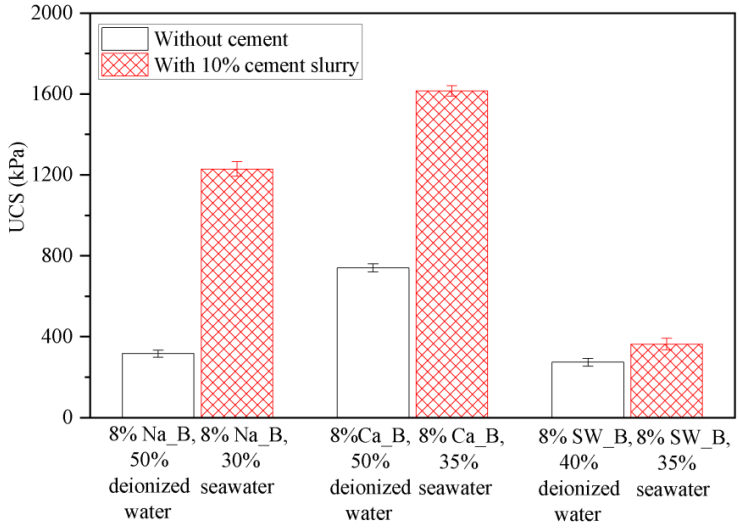

Figure 6. Unconfined compressive strength of cement-bentonite-sand mixtures at 56 days

The permeability of cement-bentonite-sand mixtures at 56 days is shown in Figure 7. The permeability of Na_B or Ca_B mixtures was lower than 10^{-8} m/s, which is commonly used as the design value for seepage cut-off walls (Wu et al., 2021). For comparison, SW_B

mixture showed the highest permeability and obtained a permeability larger than 10^{-8} m/s when 40% deionized water was used. Under comparable workability, the permeability of cement-seawater bentonite-sand mixtures were 22-592 times greater than that of the corresponding Ca_B mixtures. It is found that the seawater- and deionized water-blended Na_B mixtures show approximating permeability when different amounts of water was used. A similar observation was also noticed for Ca_B mixture. Since a lower water content means a smaller void ratio, it indicates that seawater might alter the microstructure of cemented mixture, leading to the presence of more connected pores.

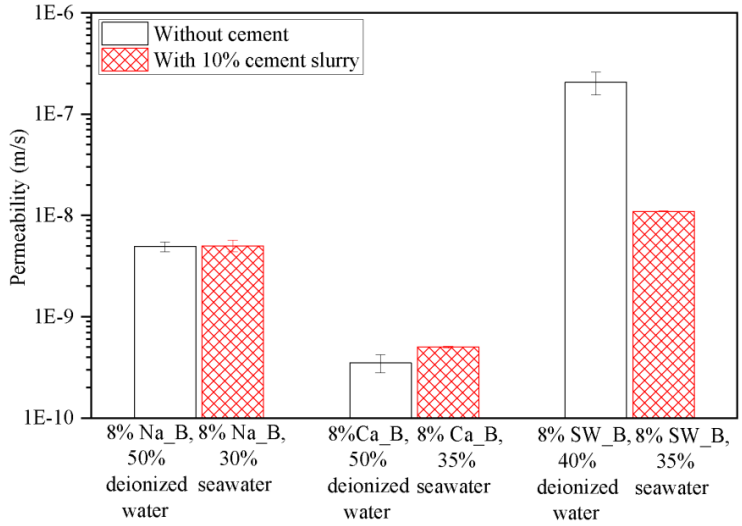

Figure 7. Permeability of cement-bentonite-sand mixtures at 56 days

3.3 Atterberg limits

To quantitatively evaluate the water-retaining capacity of bentonites, their Atterberg limits were measured with the use of deionized water, seawater, and cement slurry. Table 4 showed a remarkable decrease in the liquid limit of Na_B and Ca_B when deionized water was replaced by seawater. While for SW_B, its liquid limit also decreased with seawater, but this decrease was less prominent compared with that of Na_B and Ca_B, e.g., 28% compared with 290% and 107%. This is consistent with the variation in flowability and bleeding results of these mixtures. The reduced liquid limit should be attributed to the seawater-contained ions, as the cation exchange leads to the shrinking of diffuse double layer (DDL) of bentonite (Chen et al., 2021), resulting in a reduced inter-particle distance

and hence the decreased liquid limit, i.e., the water-retaining capacity. This is responsible for the increased flow value and bleeding rate. For the bentonite-based cut-off walls, adding cement slurry further reduced the liquid limit of bentonite, which agrees well with workability results in Figure 4 and 5.

The plastic limit of bentonite also changed with seawater incorporation. Compared with liquid limit, the changing magnitude in plastic limit is relatively small, and the plastic limit of SW_B even slightly increased when mixed with seawater. Hence, seawater intrusion led to a significantly reduced plasticity index (Table 4) of bentonites, converting the mixture from high-plasticity soil to relatively low-plasticity soil. As a result, bentonite-based mixtures may transfer from a plastic state to a liquid form with only a slight increase in water content, which poses a significant challenge to the constructability of cut-off walls.

Table 4. Atterberg limits of three bentonites

Atterberg limits	Testing medium	Bentonite type		
		Na_B	Ca_B	SW_B
Liquid limit (%)	Deionized water	403	242	204
	Seawater	113	135	176
	Deionized water and cement	86	102	86
	Seawater and cement	55	64	79
Plastic limit (%)	Deionized water	58	43	87
	Seawater	57	40	105
	Deionized water and cement	54	42	71
	Seawater and cement	48	43	77
Plasticity index (%)	Deionized water	345	199	117
	Seawater	56	95	71
	Deionized water and cement	31	60	15
	Seawater and cement	8	21	3

3.4 Scanning electron microscopy (SEM)

The SEM images (Figure 8) revealed distinct differences between the microstructure of these three bentonites after being mixed with deionized water, seawater, and cement slurry. For Na_B and Ca_B mixed with deionized water, packed flake structures were observed

with several open-air voids. In contrast, when these bentonites were mixed with seawater, aggregation of bentonite particles was observed, and bentonite particles stuck or entangled with precipitated salt. This indicated that seawater incorporation disrupts the network arrangement of bentonite particles. While for SW_B, it consisted of compacted irregular-shape particles (Figure 9c), and minor changes were observed in its morphological structure with the use of deionized water and seawater. The microstructure alternations of these bentonites are consistent with the Atterberg limits results. When cement slurry was added, bentonite particles became bonded or bridged, leading to the compacted microstructure with floccules. This should be attributed to the binding effects of hydration materials. The SEM analysis confirmed that the microstructure morphology of SW_B was less affected by seawater. However, when cement slurry was added, large flocculates consisting of SW_B particles and hydrates were noticed. As shown in Figure 8, similar morphology was noticed for bentonite-sand-bentonite mixtures, regardless of bentonite types.

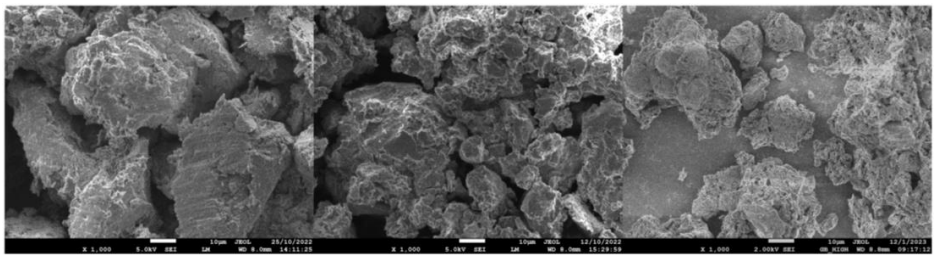

Na_B+deionized water Na_B+seawater Na_B+seawater+cement

(a)

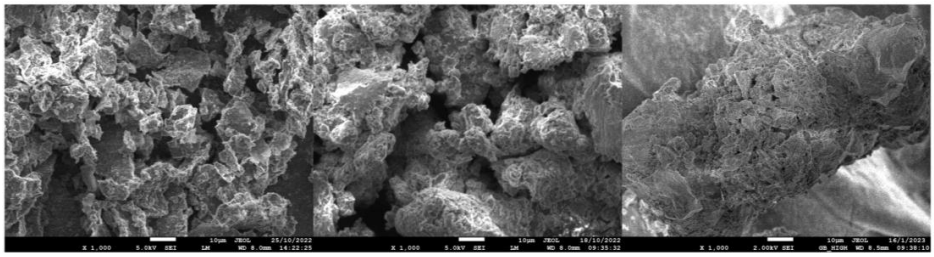

Ca_B+deionized water Ca_B+seawater Ca_B+seawater+cement

(b)

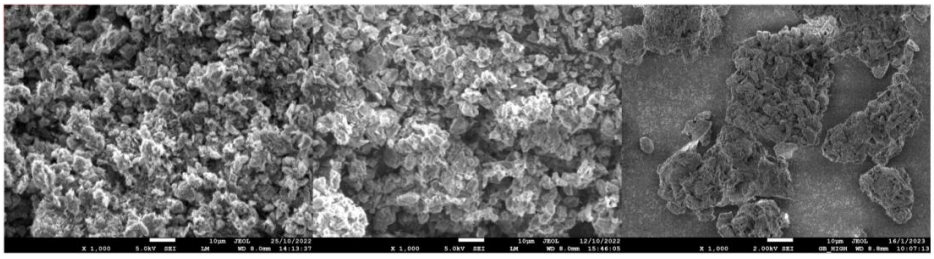

(c)

Figure 8. SEM images of bentonites with addition of deionized water/seawater and cement slurry: (a) Na_B, (b) Ca_B, and (c) SW_B

3.4 X-ray diffraction (XRD)

The clay mineral evolution of bentonites after being conditioned in deionized water, seawater, and cement slurry was evaluated by XRD technique. As shown in Figure 9, the main components of Na_B were montmorillonite and albite. The diffraction spectrum of seawater-mixed Na_B showed a shift in the montmorillonite reflection from 2θ=9.04° to 2θ=8.46° in comparison to deionized water-mixed Na_B. This reflection depends on the interlayer cation type of montmorillonite, and the montmorillonite peak at 2θ=9.04° had a basal spacing of 9.8Å, which was commonly defined for Na-montmorillonite (Ahmat et al., 2016, Dean et al., 2011). Hence, this shift indicated the exchange of the Na cations to higher-valence cations in montmorillonite interlayer (Chen et al., 2019, Kaufhold et al., 2020). This contributed to a decrease in interlamellar spacing, resulting in the formation of more compacted structures (Urena et al., 2013). Additionally, the XRD patterns of NaCl were detected in the sample mixed with seawater. As for Ca_B, the change in the intensity of montmorillonite reflection at 2θ=9.8° was also noticed. Additionally, montmorillonite peaks near 20° and 35° remained well-defined, indicating that minor alternation of the crystalline montmorillonite structure. For Na_B and Ca_B used in this study, XRD analysis confirmed the degradation of montmorillonite minerals because of the seawater-induced cation exchange reactions. When cement slurry was introduced, the intensity of montmorillonite reflections further decreased or even became discernible, indicating alterations in crystallinity owing to interactions between cement and montmorillonite.

Additionally, the reflections of NaCl became less evident after adding cement slurry, indicating the consumption of NaCl due to cement hydration.

For SW_B, the peaks of palygorskite were clearly detected and hence fewer montmorillonite peaks were observed in Figure 10c. Palygorskite is a magnesium-alumina-silicate clay mineral with high salt-resistance ability (Baltar et al., 2009). The involvement of palygorskite in seawater bentonite reduced the montmorillonite content, resulting in its lower liquid limit compared with sodium and calcium bentonites (Table 4). As for SW_B, the inflections of montmorillonite at 2θ = 20.0°, 30.9°, and 34.3° were still observed after seawater addition with a minor reduction in intensity. When cement slurry was involved, the montmorillonite inflections became discernible, and the intensity of palygorskite decreased significantly, indicating the degradation and structural distortion. This is responsible for the significant change in the workability of SW_B mixture after adding cement slurry.

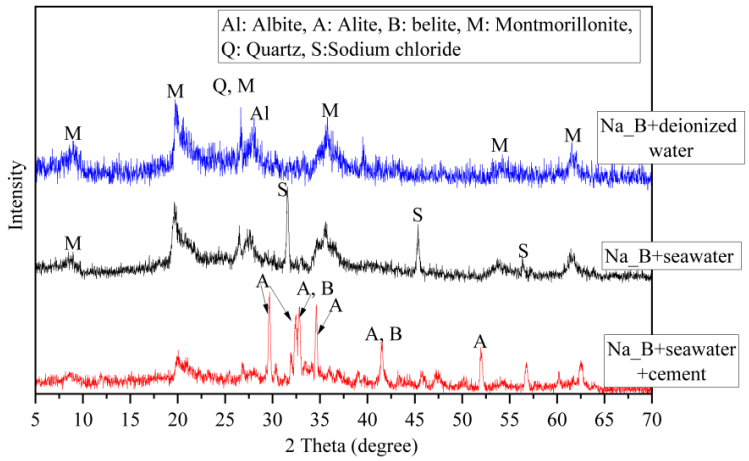

(a)

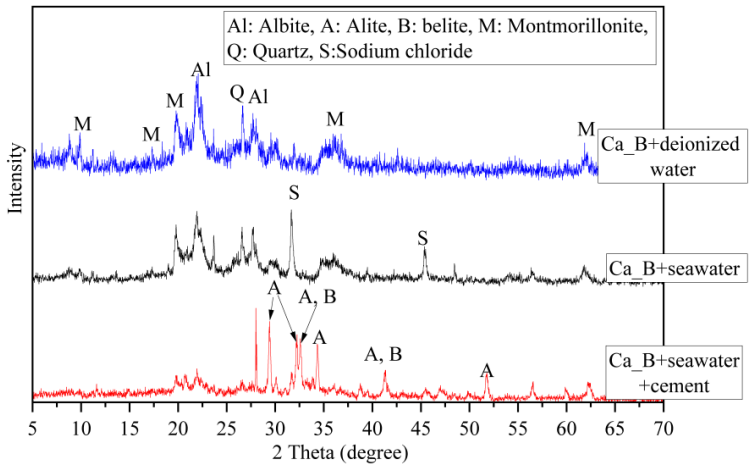

(b)

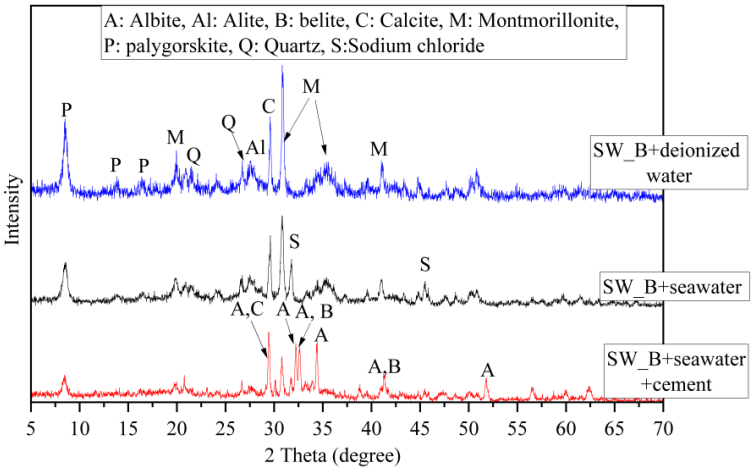

(c)

Figure 9. XRD patterns of bentonites with addition of deionized water/seawater and cement slurry: (a) Na_B, (b) Ca_B, and (c) SW_B

3.5 Fourier Transform Infrared (FTIR)

FTIR analysis was conducted to characterize the vibrational properties of the soil mineralogy of the bentonites. As shown in Figure 10, the observed band at 3624 cm^{-1} for both Na_B and Ca_B is associated with structural -OH groups in montmorillonites. When seawater was used, the -OH stretching bands shifted respectively. Impurities in Ca_B were identified, including dolomite at 1430 cm^{-1} and quartz at about 796 cm^{-1} (Frankovská et al., 2010). For absorption bands in this region, none or minor changes were detected in the

373 FTIR spectrums of Na_B and Ca_B after the addition of seawater or cement slurry. The
374 water molecule in bentonite was detected by the broad peak observed at 1634 cm^{-1} (Bishop
375 et al., 1994). When bentonite was mixed with seawater, the water band at ~3400 cm^{-1} was
376 detected because of the overlapping of asymmetric and symmetric H-O-H stretching
377 vibrations (Madejová et al., 2002). Additionally, the bands of Al-Al-OH, Al-Fe-OH, and
378 Fe-Mg-OH minerals in montmorillonite were identified at 916, 876, and 786 cm^{-1},
379 respectively (Motawie et al., 2014, Vantelon et al., 2001). The vibrations of -OH groups at
380 these regions suggested the substitution of Al octahedral by Fe and Mg (Alazigha et al.,
381 2018). For Na_B, the bands of Si-O-Si at 992 cm^{-1}, expanded and moved to around 1002
382 cm^{-1} after incorporating seawater and cement slurry, indicating the change of Si-O groups
383 in montmorillonite structure (Alves et al., 2016). Similar alternations were observed for the
384 Si-O-Si reflection of Ca_B at 999 cm^{-1}. The band at 1634 cm^{-1} became intensified after
385 seawater addition, which was caused by the hydration of H-O-H bending (Baú et al., 2020).
386
387 While for SW_B, the detected bands at 3616 cm^{-1} are well related to the OH bands in
388 montmorillonite (Frankovská et al., 2010). Typical bands of palygorskite at 3616, 3544,
389 and 1196 cm^{-1} remained constant after seawater addition, confirming the negligible effect
390 of seawater on the palygorskite structure. Nonetheless, as indicated in Figure 10, the
391 intensity of these bands decreased after cement slurry addition, confirming the dissolution
392 of palygorskite. Additionally, the Al–O–Si stretching band at about 976 cm^{-1} slightly
393 decreased its intensity after seawater and cement slurry addition, indicating alternation in
394 montmorillonite structure.

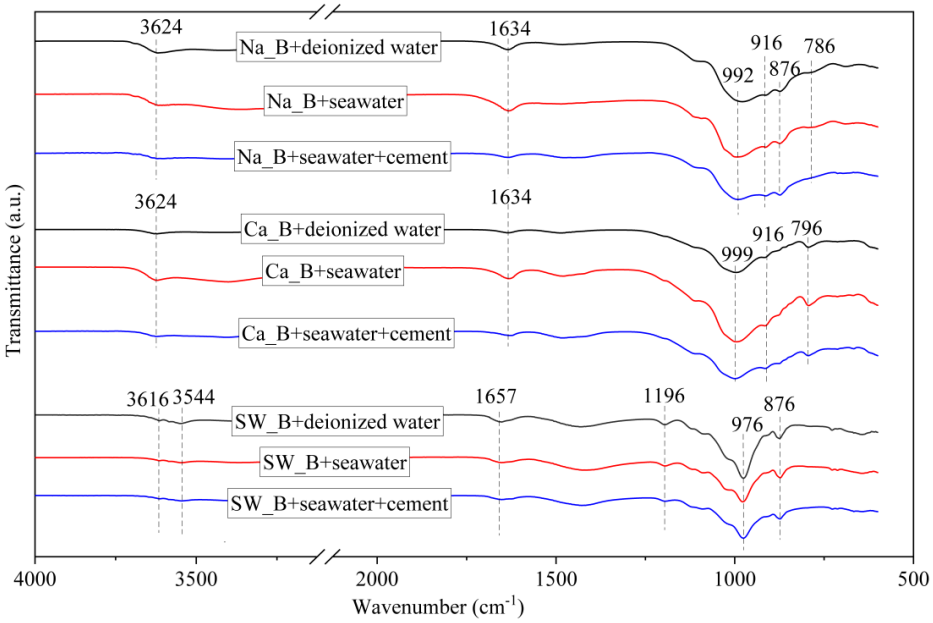

Figure 10. FTIR curves of bentonites mixed with deionized water/seawater or cement slurry

4. Discussion

The experimental results show that seawater significantly increased the workability of sand bentonite mixture and narrowed the workable water content range, especially for the Na_B and Ca_B mixture. The workability of SW_B mixture was less affected by seawater; however, when cement was added, SW_B mixture showed a remarkable increment in workability and yielded lower strength and higher permeability than those of the Na_B and Ca_B mixture.

The water-retaining capacity of bentonite dominates the workability of bentonite-sand mixture. XRD analysis indicated that seawater-induced cation exchange leads to the conversion of Na-montmorillonite to montmorillonite with higher-valence cations, which possess a relatively smaller thickness of DDL (Mishra et al., 2009). Hence, seawater lowered the water-retaining capacity of bentonite, as indicated by the decreased liquid limit (Table 4). SEM images further confirmed the particle aggregation and rheology modification of bentonite particles after seawater addition (Figure 8). Among these

bentonites, SW_B was less impacted by seawater owing to its lowest quantity of exchangeable sodium ions (Table 1) and the high content of palygorskite. Additionally, the change in Atterberg limits led to a significantly reduced plasticity index of Na_B and Ca_B, converting the mixture from high-plasticity soil to low-plasticity soil (Table 4). As shown in Figure 11, a remarkable reduction in the workable water content range was noticed for the Na_B and Ca_B mixture when incorporating seawater, e.g., 60%-79% reduced to 33%-41% for mixtures with 12% Na_B, while that of the SW_B mixture was insignificant. Therefore, bentonite-based mixtures can readily surpass the workability requirement with a slight increase in water content, posing challenges to the constructability.

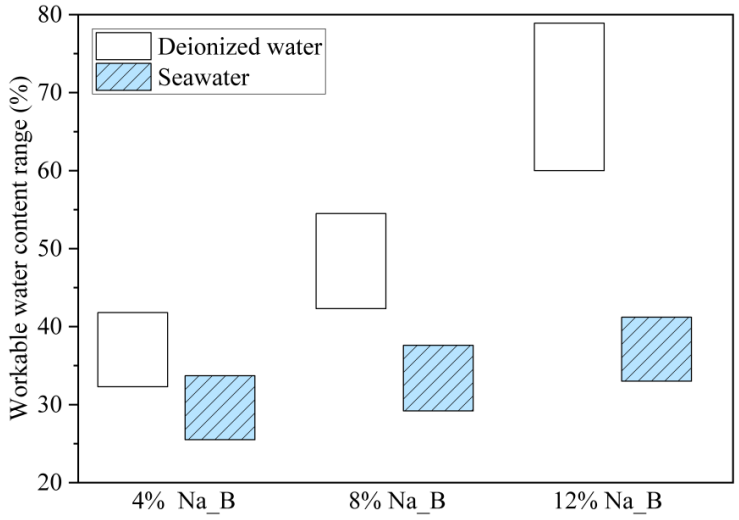

(a)

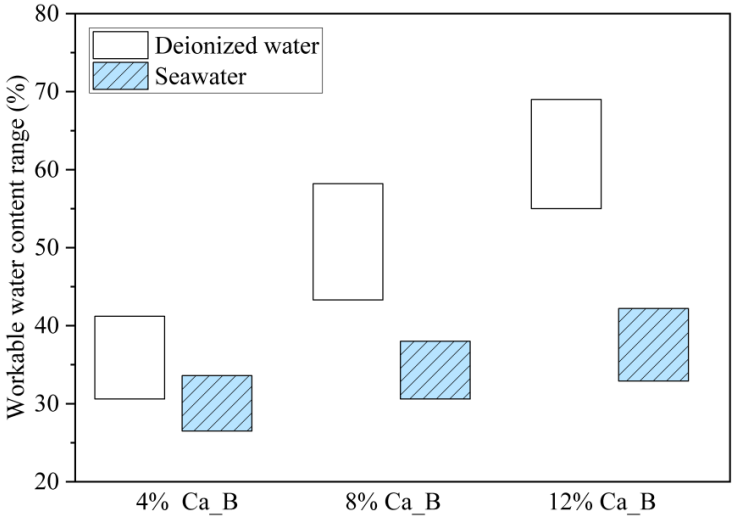

(b)

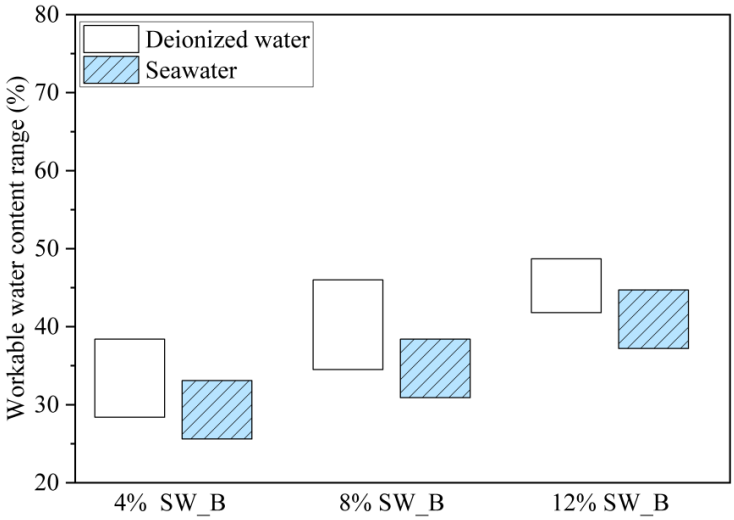

(c)

Figure 11. Workable water content range of bentonite-sand mixtures with seawater and deionized water: (a) Na_B, (b) Ca_B, and (c) SW_B

Adding cement slurry to bentonite-sand mixtures further increased the flowability, and this effect is more prominent in seawater environment. This can be attributed to the facilitated cement hydration rate within a seawater environment (Ting and Yi, 2023), leading to the release of more Ca^{2+} ions and further promoting the cation exchange. The cations adsorbed on bentonite exhibited a replaceable pattern in a preferential sequence, with Na^{+} being

436 replaced first, followed by K^+, Mg^{2+}, and Ca^{2+}, owing to the rise in atomic valence energy
437 (Camillis et al., 2016, Komine et al., 2009). The cation exchange processes are illustrated
438 in Figure 12. Hence, cement addition further decreased the liquid limit of bentonite.
439 Compared with Na_B and Ca_B mixtures, SW_B mixtures showed the highest increment
440 in workability after adding cement slurry. This is because cement addition leads to the
441 decomposition of palygorskite, which dissolved quickly in a high-pH environment, as
442 confirmed by the XRD and FTIR analyses.

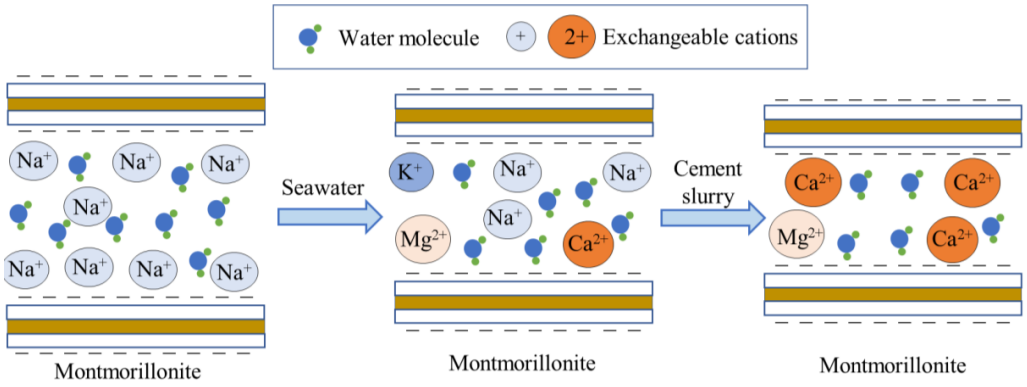

443

444 **Figure 12.** Schematic illustration of cation exchange of bentonite with seawater and
445 cement slurry

446

447 For cement-bentonite-sand mixtures containing either Na_B or Ca_B, seawater lowered
448 the initial water content by 10%-15% for obtaining a workable flowability and promoted
449 cement hydration, leading to a higher strength. Moreover, bentonite-sand cement mixtures
450 prepared with seawater exhibited lower initial water content but similar permeability
451 compared with those prepared using deionized water, regardless of whether sodium or
452 calcium bentonite was used. Since the seawater-prepared mixtures had an initial water
453 content 10%-15% lower than that of the deionized water mixtures, it is indicated that there
454 are more connected pores in the seawater-prepared mixtures. For SW_B mixtures,
455 preparing them in a seawater environment yielded slightly higher strength and lower
456 permeability than those of the deionized water counterparts. Figure 8 showed that the
457 seawater had minor effects on the microstructure of SW_B; hence, the difference in water
458 content should be the reason for the variations in strength and permeability. Cement-
459 bentonite-sand mixture prepared with Ca_B achieved the highest compressive strength and

the lowest permeability. For comparison, the strength of SW_B mixtures was 63%-78% lower than that of Ca_B mixtures, depending on the water type. This may be because the magnesium component in SW_B reacts with cementitious materials to form magnesium hydroxide and non-cementing MSH (Bernard et al., 2019), and hence the low strength. For bentonites used in this study, the cost of Ca_B was 64% and 42% that of Na_B and SW_B, respectively. Therefore, Ca_B would be a preferable choice for the construction of cement-bentonite-sand cut-off walls in coastal regions.

In summary, seawater-induced cation exchanges are the primary mechanism responsible for the increased workability of bentonite-based cut-off walls, resulting in a narrowed workable water content range. Compared with Na_B and Ca_B, SW_B is less affected by seawater, but its water-retaining capacity decreased significantly upon exposure to cement. The findings emphasized the critical role of bentonite minerals and their properties in reducing the impact of cation exchange. In subsequent research, attention will be given to investigating the interactions between binders and bentonite, as well as identifying suitable binders for the construction of cut-off walls in marine regions.

5. Conclusions

The effects of seawater on bentonite-based seepage cut-off walls with and without addition of cement have been studied via laboratory experiments. Main conclusions are drawn as follows:

1. The flowability and bleeding of bentonite-sand mixtures increased after the incorporation of seawater, which was caused by the reduced water-retaining capacity of bentonite. Sodium bentonite showed the highest reduction in liquid limit, i.e., 290%, while that of calcium bentonite and seawater bentonite were 107% and 28%, respectively. The plastic limit of bentonite was less affected by seawater, resulting in a reduced workable water content range of bentonite-sand mixtures.

2. The addition of cement slurry further increased the flowability and bleeding of fresh bentonite-sand mixtures. Seawater bentonite can maintain its water-retaining capacity in a seawater environment, but showed the largest increment in flowability and bleeding upon cement addition.

3. XRD result revealed the conversion of montmorillonite type due to cation exchange, which depressed the interlayer spacing of bentonite and reduced its ability to retain water. SEM analysis confirmed the flocculated morphology of bentonite particles with addition of seawater and/or cement slurry.

4. Under comparable workability, the calcium bentonite-sand-cement mixture achieved the highest strength and the lowest permeability. For comparison, the strength and permeability of the seawater bentonite-sand-cement mixture were 63%-78% lower and 22-592 times higher than those of the calcium bentonite-sand-cement mixture, respectively.

5. The bentonite-sand-cement mixtures prepared with seawater exhibited lower initial water content but similar permeability compared with those prepared using deionized water, regardless of whether sodium or calcium bentonite was used. This suggests the presence of more connected pores in the seawater-mixed mixtures.

Acknowledgments

This research was supported by the Ministry of Education, Singapore, under its Academic Research Fund Tier 2 (MOE-T2EP50220-0004). The authors also acknowledge the supports from The National Natural Science Foundation of China (Grant No. 5230080603) and The Natural Science Foundation of the Jiangsu Higher Education Institutions of China (Grant No. 23KJB560023).

REFERENCES

Ahmat, A. M., Boussafir, M., Le Milbeau, C., Guegan, R., Valdès, J., Guiñez, M., Sifeddine, A. & Le Forestier, L. (2016) Organic matter-clay interaction along a seawater column of the Eastern Pacific upwelling system (Antofagasta bay, Chile): Implications for source rock organic matter preservation. *Marine Chemistry* **179**:23-33.

Alazigha, D. P., Indraratna, B., Vinod, J. S. & Heitor, A. (2018) Mechanisms of stabilization of expansive soil with lignosulfonate admixture. *Transportation Geotechnics* **14**:81-92.

Alves, J. L., Rosa, P. D. T. V. & Morales, A. R. (2016) A comparative study of different routes for the modification of montmorillonite with ammonium and phosphonium salts. *Applied Clay Science* **132**:475-484.

ASTM. (2007)Standard test methods for compressive strength of molded soil-cement cylinders. West Conshohocken, PA.

ASTM. (2010)Standard test methods for measurement of hydraulic conductivity of saturated porous materials using a flexible wall permeameter. West Conshohocken, PA.

ASTM. (2016)Standard test method for expansion and bleeding of freshly mixed grouts for preplaced-aggregate concrete in the laboratory. West Conshohocken, PA.
ASTM. (2017)Standard test methods for liquid limit, plastic limit, and plasticity index of soils. West Conshohocken, PA.
ASTM. (2018)Standard test method for measuring the exchange complex and cation exchange capacity of inorganic fine-grained soils. West Conshohocken, PA.
Baltar, C. a. M., Da Luz, A. B., Baltar, L. M., De Oliveira, C. H. & Bezerra, F. J. (2009) Influence of morphology and surface charge on the suitability of palygorskite as drilling fluid. *Applied Clay Science* **42(3-4)**:597-600.
Baú, J. P. T., Villafañe, S. A., Da Costa, A. C. S., Negrón, A., Colín, M. & Zaia, D. A. (2020) Adenine adsorbed onto montmorillonite exposed to ionizing radiation: Essays on prebiotic chemistry. *Astrobiology* **20(1)**:26-38.
Bernard, E., Lothenbach, B., Chlique, C., Wyrzykowski, M., Dauzeres, A., Pochard, I. & Cau-Dit-Coumes, C. (2019) Characterization of magnesium silicate hydrate (MSH). *Cement and Concrete Research* **116**:309-330.
Bishop, J. L., Pieters, C. M. & Edwards, J. O. (1994) Infrared spectroscopic analyses on the nature of water in montmorillonite. *Clays and clay minerals* **42**:702-716.
Boesch, D. F., Boicourt, W., Cullather, R., Ezer, T., Galloway Jr, G., Johnson, Z., Kilbourne, K., Kirwan, M., Kopp, R. & Land, S. (2018) *Sea-level rise: projections for Maryland 2018*.
Camillis, M. D., Emidio, G. D., Bezuijen, A. & Verástegui-Flores, R. D. (2016) Hydraulic conductivity and swelling ability of a polymer modified bentonite subjected to wet–dry cycles in seawater. *Geotextiles and Geomembranes* **44(5)**:739-747.
Chen, Y., Cai, Y., Pan, K., Ye, W. & Wang, Q. (2021) Influence of dry density and water salinity on the swelling pressure and hydraulic conductivity of compacted GMZ01 bentonite–sand mixtures. *Acta Geotechnica*:1-18.
Chen, Y., Sun, Z., Cui, Y., Ye, W. & Liu, Q. (2019) Effect of cement solutions on the swelling pressure of compacted GMZ bentonite at different temperatures. *Construction and Building Materials* **229**:116872.
Cheng, H., Li, W., Chen, R. & Yi, Y. (2022) Workability study of sand-bentonite-cement mixtures for construction of two-phase cut-off wall. *Construction and Building Materials* **345**:128058.
Choupani, M., Tabatabaee Moradi, S. & Tabatabaei Nejad, S. (2022) Study on attapulgite as drilling fluid clay additive in Persian Gulf seawater. *International Journal of Engineering* **35(3)**:587-595.
Cui, J., Zhang, Z. & Han, F. (2020) Effects of pH on the gel properties of montmorillonite, palygorskite and montmorillonite-palygorskite composite clay. *Applied Clay Science* **190**:105543.
Dean, K. M., Petinakis, E. & Yu, L. (2011) Biodegradable thermoplastic starch/poly (vinyl alcohol) nanocomposites with layered silicates. *Nanocomposites with Biodegradable Polymers: Synthesis, Properties, and Future Perspectives* **68**:58.
Evans, J. C. (2007) The TRD method: slag-cement materials for in situ mixed vertical barriers. In *Soil Improvement*.), pp. 1-11.
Evans, J. C. & Garbin, E. J. (2009) The TRD method for in situ mixed vertical barriers. In *Advances in Ground Improvement: Research to Practice in the United States and China*.), pp. 271-280.
Frankovská, J., Andrejkovičová, S. & Janotka, I. (2010) Effect of NaCl on hydraulic properties of bentonite and bentonite–palygorskite mixture. *Geosynthetics International* **17(4)**:250-259.
JCJ/T303. (2013)Technical specification for trench cutting remixing deep wall. Beijing, China, China Building Industry Press.
Kaufhold, S., Dohrmann, R. & Ufer, K. (2020) Determining the extent of bentonite alteration at the bentonite/cement interface. *Applied Clay Science* **186**:105446.

576 Komine, H., Yasuhara, K. & Murakami, S. (2009) Swelling characteristics of bentonites in artificial
577 seawater. *Canadian Geotechnical Journal* **46(2)**:177-189.
578 Kumar, A., Veluswamy, H. P., Kumar, R. & Linga, P. (2019) Direct use of seawater for rapid
579 methane storage via clathrate (sII) hydrates. *Applied Energy* **235**:21-30.
580 Madejová, J., Janek, M., Komadel, P., Herbert, H.-J. & Moog, H. (2002) FTIR analyses of water
581 in MX-80 bentonite compacted from high salinary salt solution systems. *Applied Clay*
582 *Science* **20(6)**:255-271.
583 Mishra, A. K., Ohtsubo, M., Li, L. Y., Higashi, T. & Park, J. (2009) Effect of salt of various
584 concentrations on liquid limit, and hydraulic conductivity of different soil-bentonite
585 mixtures. *Environmental geology* **57**:1145-1153.
586 Motawie, A., Madany, M., El-Dakrory, A., Osman, H., Ismail, E., Badr, M., El-Komy, D. &
587 Abulyazied, D. (2014) Physico-chemical characteristics of nano-organo bentonite prepared
588 using different organo-modifiers. *Egyptian journal of petroleum* **23(3)**:331-338.
589 Norris, A., Di Emidio, G., Malusis, M. A. & Replogle, M. (2018) Modified bentonites for soil-
590 bentonite cutoff wall applications with hard mix water. *Applied Clay Science* **158**:226-235.
591 Shi, F., Feng, S., Zheng, Q., Zhang, X. & Chen, H. (2022) Effect of polyanionic cellulose
592 modification on properties and microstructure of calcium bentonite. *Applied Clay Science*
593 **228**:106633.
594 Ting, M. Z. Y. & Yi, Y. (2023) Durability of cementitious materials in seawater environment: A
595 review on chemical interactions, hardened-state properties and environmental factors.
596 *Construction and Building Materials* **367**:130224.
597 Urena, C., Azanon, J., Corpas, F., Nieto, F., Leon, C. & Perez, L. (2013) Magnesium hydroxide,
598 seawater and olive mill wastewater to reduce swelling potential and plasticity of bentonite
599 soil. *Construction and Building Materials* **45**:289-297.
600 Vantelon, D., Pelletier, M., Michot, L. J., Barres, O. & Thomas, F. (2001) Fe, Mg and Al
601 distribution in the octahedral sheet of montmorillonites. An infrared study in the OH-
602 bending region. *Clay Minerals* **36(3)**:369-379.
603 Vernimmen, R. & Hooijer, A. (2023) New LiDAR-based elevation model shows greatest increase
604 in global coastal exposure to flooding to be caused by early-stage sea-level rise. *Earth's*
605 *Future* **11(1)**:e2022EF002880.
606 Wu, H., Jin, F., Zhou, A. & Du, Y. (2021) The engineering properties and reaction mechanism of
607 MgO-activated slag cement-clayey sand-bentonite (MSB) cutoff wall backfills.
608 *Construction and Building Materials* **271**:121890.
609 Ying, Z., Cui, Y., Duc, M., Benahmed, N., Bessaies, H. & Chen, B. (2021) Salinity effect on the
610 liquid limit of soils. *Acta Geotechnica* **16**:1101-1111.

611

612